Available online at www.sciencedirect.com
SCIENCE DIRECT
ELSEVIER
Journal of Solid State Chemistry 177 (2004) 1639–1645
JOURNAL OF SOLID STATE CHEMISTRY
http://elsevier.com/locate/jssc

Fabrication of crystallized boron films by laser ablation

Zhongke Wang,[a] Yoshiki Shimizu,[a] Takeshi Sasaki,[a] Kazuhiro Kirihara,[a] Kenji Kawaguchi,[a] Kaoru Kimura,[b] and Naoto Koshizaki[a,*]

[a] *Nanoarchitectonics Research Center (NARC), National Institute of Advanced Industrial Science and Technology (AIST), Central 5, 1-1-1 Higashi, Tsukuba, Ibaraki 305-8565, Japan*

[b] *Department of Advanced Materials Science, Graduate School of Frontier Sciences, The University of Tokyo, Kiban-toh 502, 5-1-5 Kashiwanoha, Kashiwa, Chiba 277-8651, Japan*

Received 14 October 2003; received in revised form 1 December 2003; accepted 14 December 2003

Abstract

Polycrystalline β-rhombohedral boron films mixed with amorphous boron phase have been successfully fabricated on quartz substrates using pulsed laser ablation in a quartz glass tube chamber placed in an electric furnace. The crystallinity of the films strongly depended on the temperature of the furnace and the pressure of background argon gas. High temperature and high pressure in the chamber were suitable for crystallized boron film preparation. The best crystalline films (without B_2O_3 phase formation) were obtained at 1000°C, 100 Pa. XPS measurements demonstrated that the major contaminants were carbon and oxygen, and the atomic ratio of oxygen to boron was 0.05 under the preparation conditions of well-crystallized films. The surface roughness of the films decreased by lowering laser energy to 150 mJ/pulse under the same pressure and temperature conditions.
© 2003 Elsevier Inc. All rights reserved.

Keywords: β-rhombohedral boron; Crystallized film; Laser ablation; Growth mechanism

1. Introduction

Thermoelectric energy conversion is a very reliable way of generating electrical power, for example from solar heat or from waste industrial thermal energy. Boron and boron-rich solids are very promising candidates for high efficiency thermoelectric energy conversion. The high mechanical strength, and high melting points allow their use under extreme conditions that are not accessible by other materials. Previous research revealed that boron and some boron-rich semiconductors exhibited very favorable transport properties such as electrical conductivity of typical semiconductors and very low thermal conductivity [1–4]. However, it is difficult to prepare pure, highly crystallized boron films. An earlier study demonstrated that films fabricated by the magnetron sputtering method were amorphous [5]. The chemical vapor deposition (CVD) method has been the most widely studied technique for crystallized boron film preparation, although it generally required high temperature and hazardous chemicals. For example, crystalline boron films were often fabricated by thermal reduction of boron trichloride or other boron halides using hydrogen [6–12], by pyrolysis of decaborane ($B_{10}H_{14}$) in vacuum [3,13], or by thermal decomposition of diborane (B_2H_6) at low pressure [4,14]. Films grown at a temperature range of 700–1050°C were amorphous, while those grown at a substrate temperature of 1150°C became a mixture of amorphous and polycrystalline phases [4]. In a substrate temperature range of 1100–1250°C, α-rhombohedral boron was obtained in a hot-wire fiber growth CVD reactor [12]. No deposition of boron was observed below 750°C in the dual impinging-jet CVD reactor [15].

The laser ablation technique does not require such gaseous raw materials as in the CVD method, and offers the advantages of simplicity, versatility, and experimental ease [16,17]. Modest substrate temperatures due to high energy of the ejected species are also possible for this technique. Therefore, laser ablation has been widely used for the deposition of dielectrics, superconductors, semiconductors, and other materials, despite the potential production of "droplet" during laser ablation [16,18–21]. We recently succeeded in preparing crystallized

*Corresponding author. Fax: +81-29-861-6355.
E-mail address: koshizaki.naoto@aist.go.jp (N. Koshizaki).

0022-4596/$ - see front matter © 2003 Elsevier Inc. All rights reserved.
doi:10.1016/j.jssc.2003.12.018

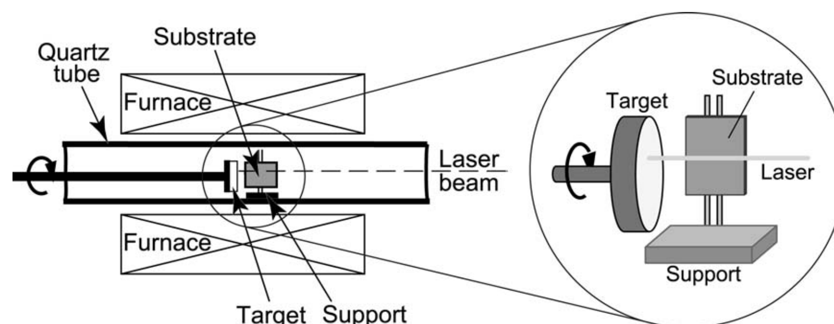

Fig. 1. Experiment setup for boron film preparation by laser ablation.

boron nanobelts using the laser ablation technique [22]. In this case, nanobelts were crystallized in α-tetragonal structure that is different from the most common crystalline boron phase of α- or β-rhombohedral structure. However, we sometimes found a crystallized boron film during the study of boron nanobelts at relatively low temperatures of 700–900°C. In this article, we report the preparation of crystallized boron films by laser ablation in furnace, especially focusing on the processing parameter dependence on film crystallinity, composition, and morphology.

2. Experimental

We used a quartz glass tube placed in an electric furnace as a chamber for the laser ablation. Fig. 1 schematically illustrates the experiment apparatus. A compressed pure boron pellet target (about 65% in relative density, 99.5% pure, purchased from Japan Pure Chemical Co., Ltd.) was mounted on a rotating holder in the chamber, and placed at the center of the tube in the furnace. A quartz glass substrate was situated perpendicularly at the side of the tube, where particles or belt-like structures from the target can be prevented from depositing on the substrate surface. In our previous study on boron nanobelt fabrication by laser ablation, the nanobelts were deposited on the substrate surface placed on the bottom of the tube during the ablation process [22]. The temperature at the center of the tube chamber can be controlled up to 1100°C.

Laser ablation was performed using a third harmonic Nd:YAG laser (wavelength = 355 nm, pulse width = 5–7 ns, repetition = 10 Hz). The laser energy for ablation was 50–250 mJ/pulse, with a spot size of 3.2 mm^2. The target surface was irradiated through a quartz glass window of the chamber. The ablation chamber was evacuated by a rotary pump before the experiments, and Ar gas was introduced at five standard cubic centimeters per minute (sccm) in a pressure range of 20–300 Pa.

We measured the thickness of obtained films by a profilometer (Tencor alpha-step profiler 300) and a field emission scanning electron microscope (FE-SEM, Hitachi S-4800). The films were about 5 μm thick after 60 min deposition, though the thickness was not uniform throughout the entire film. The crystal structure of the films was analyzed by X-ray diffraction (XRD, Rigaku RAD-C) using Cu*K*α radiation. High-resolution transmission electron microscopic (HR-TEM, JEOL JEM-2010, 200 kV) observation was performed for detailed structural characterization of the boron films. Boron powders peeled from the substrate were dispersed ultrasonically in acetone, and the resultant solution was dropped on a copper grid covered with holey carbon film for TEM observation. The surface morphology of the films was observed by FE-SEM. We also characterized the compositions of the films and the chemical state of constituent elements by X-ray photoelectron spectroscopy (XPS, PHI 5600ci), after sputtering for 15 min to remove surface contamination. Chemical state analyses were performed by taking binding energy of B1s main peak as 187.3 eV for charge-up correction [23].

3. Results and discussion

3.1. XRD analysis

Fig. 2 depicts the typical XRD spectra of films deposited at 100 Pa with 250 mJ/pluse under different temperatures. The broad hump seen at the lower angle near 22° was from the amorphous quartz substrate. The strongest peak, observed at 17.6°, corresponded to the (1 0 4) peak of β-rhombohedral boron. The peak intensity and the number of peaks observed in the spectra increased with the ambient temperature from 600°C to 1000°C. However, the peak width did not significantly change, indicating no crystallite size increase with temperature.

We adopted the intensity ratio I_B/I_g of the XRD peak from crystallized boron, I_B, to that of SiO_2 substrate, I_g, as a measure to evaluate the film crystallinity, as depicted in Fig. 3. This value is a convolution of crystallization of the film and the film thickness, since

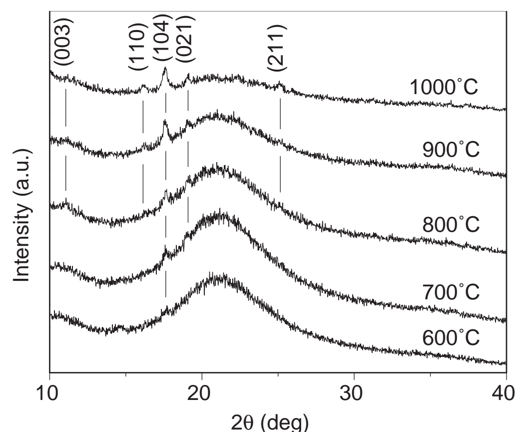

Fig. 2. XRD spectra of boron films deposited at 100 Pa using 250 mJ/pulse at various temperatures.

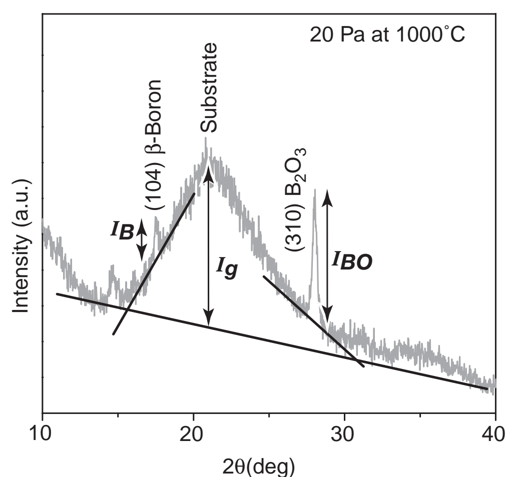

Fig. 3. Procedure for estimating crystallinity of β-boron and boron oxide from the XRD spectrum of the film deposited on quartz substrate under various conditions. Intensity ratios of I_B/I_g and I_{BO}/I_g were used as measures of crystallinity and oxidation of films.

the thick film reduces the signal from the substrate and increases the ratio. We sometimes observed a peak at 28° from B_2O_3 (310) peak under specific conditions, and we also calculated the XRD peak intensity ratio I_{BO}/I_g in a similar way.

Fig. 4 presents the I_B/I_g XRD peak intensity ratio for various temperatures and pressures. Large dots in Fig. 4 correspond to the large peak intensity ratio I_B/I_g. The films deposited at low temperatures and low pressures (below 700°C at 50 Pa, and below 1000°C at 20 Pa) were amorphous boron, as indicated by " × " marks, while those at higher temperatures and pressures were crystalline in β-rhombohedral phase. Film crystallinity increased with substrate temperature irrespective of the difference in pressure. Crystalline films could be obtained at lower substrate temperatures by increasing the background argon gas pressure. However, a well-crystallized boron oxide peak was observed only at temperatures higher than 900°C, and the pressures lower

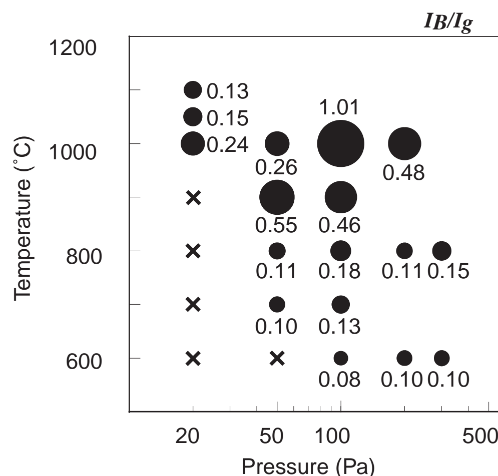

Fig. 4. Peak intensity ratio of I_B/I_g determined from XRD spectra under various temperature and pressure conditions. Dots indicate the conditions under which the crystallized boron peak was observed, and large dots indicate high peak intensity ratio of I_B/I_g. The " × " marks correspond to the conditions where no crystalline peak was observed in the deposited films.

than 100 Pa. The peak intensity ratios I_{BO}/I_g were 0.80 at 1000°C, 20 Pa, and 1.86 at 1000°C, 50 Pa. Thus, boron and boron oxide coexisted under these preparation conditions. The range of preparation conditions for crystallized boron films, amorphous boron, and coexistence of boron and boron oxide are illustrated in Fig. 5. The best fabrication condition for the crystallized β-rhombohedral boron film (without crystallized B_2O_3 formation) was 1000°C, 100 Pa out of various conditions we examined. We have to note that the crystallized boron films were generally grown above 1200°C by the CVD method [4,12], and more than 1100°C was required for crystallized nanowire preparation by CVD method [24]. The crystallized boron nanobelt formation range in our previous study is also presented in Fig. 5, although the target-substrate configurations differed from each other. The well-crystallized α-tetragonal boron nanobelts were fabricated at 20 Pa in a temperature range of 700–900°C. The yield of nanobelts greatly decreased below 700°C or above 900°C [22] even at 20 Pa. Thus, the formation ranges of crystallized β-rhombohedral boron film and crystallized α-tetragonal boron nanobelts were almost exclusive with each other.

We also performed similar experiments for boron film preparation using conventional UHV chamber (base pressure less than 10^{-8} Pa) with the same target-substrate configuration for comparison. In this case we used neither alumina tube nor silica substrate. However we hardly obtained the films without B_2O_3 XRD peak under the same pressure, or even UHV, and under the same temperature range, indicating that oxygen came possibly from residual gas or water molecule adsorbed on the inner wall of chamber. In contrast, our laser

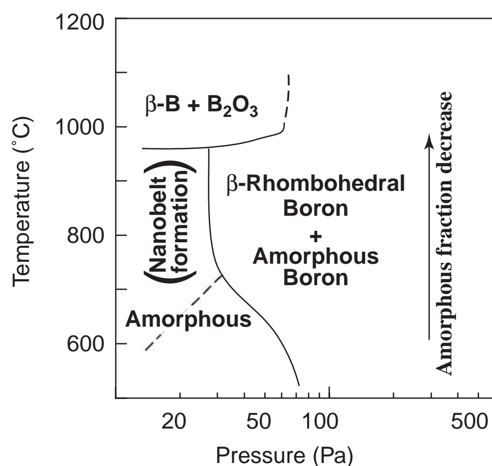

Fig. 5. Summarized preparation conditions for crystallized boron films, amorphous boron, and coexistence of boron and boron oxide. Nanobelt formation condition in our previous study is also indicated.

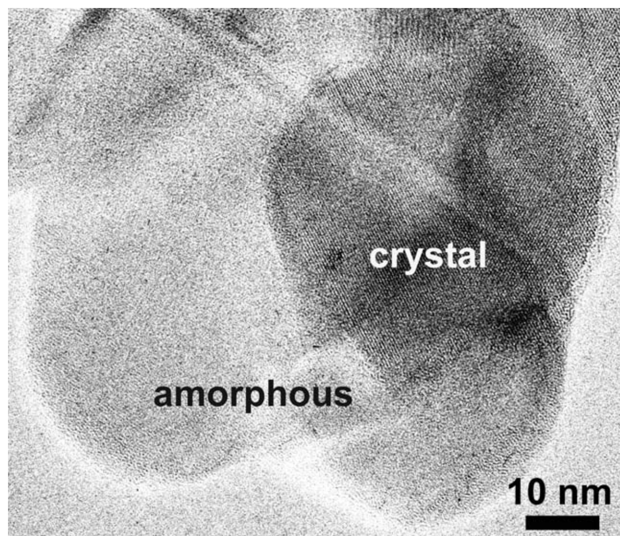

Fig. 6. HR-TEM image of typical products obtained at 800°C, 200 Pa, clearly indicating that the amorphous grains were mixed with crystal grains.

ablation technique in furnace brought less oxide films without using UHV chamber.

3.2. TEM analysis

Fig. 6 presents an HR-TEM image of the typical products obtained at 800°C, 200 Pa, indicating that the amorphous grains were mixed with crystal grains. These crystalline grains were β-rhombohedral boron, as identified from XRD and transmission electron diffraction. Additionally, we also observed some grains consisting of amorphous and crystal parts. Thus the boron films were not fully crystalline, but composed of a mixture of amorphous and crystalline phases. However, the fraction of crystallized boron in the films increased with process temperatures.

3.3. XPS analysis

Boron is a very reactive material, and hence impurity inclusion in the film is inevitable. Minimizing impurities in the prepared films is an important issue for further applications. Therefore, we analyzed the content and chemical state of impurities in the films by XPS. Fig. 7 presents a typical XPS spectra of the boron film prepared at 1000°C, 100 Pa. The inset of Fig. 7 depicts B1s peak consisting of a single component of boron. Carbon, oxygen, nitrogen, and silicon (apart from boron) were observed on the film surface. The content of these minor components, especially carbon and oxygen, was decreased by Ar sputter etching, and became almost constant after 15 min sputtering. Therefore, we determined impurity contents by XPS analyses after 15 min sputter etching. Tables 1 and 2 present O/B and C/B atomic ratios obtained under various deposition conditions. Relatively higher values of O/B atomic ratio were obtained at higher temperatures with lower pressure range where a B_2O_3 peak was observed in the XRD spectra. XPS B1s peak from B_2O_3 correspondingly appeared at 192–194 eV under these conditions [25]. However, the low oxygen content in the boron film was obtained under the conditions where the well-crystallized films were obtained, although the deposition conditions were very close to the above oxide-coexisting region. The C/B atomic ratio was high at lower deposition temperatures, and gradually decreased with the deposition temperature increase. The low carbon content in the boron film was also obtained under the same conditions for which the well-crystallized films were obtained. The chemical state of carbon contaminant can be attributed to carbide components. Nitrogen

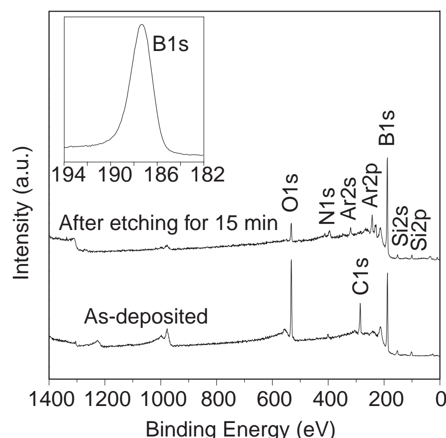

Fig. 7. Typical XPS spectra of boron film prepared at 1000°C, 100 Pa. Lower and upper curves are from the films as-deposited and after etching for 15 min. Carbon, oxygen nitrogen, and silicon were observed as contaminants of boron films. The inset depicts B1s peak consisting of a single component of boron.

Table 1
Atomic ratio O/B in boron films deposited under various conditions

Temperature (°C)	Pressure (Pa)				
	20	50	100	200	300
1050	0.18				
1000	0.05	0.12	0.05	0.09	
900	0.04	0.03	0.05		
800	0.13	0.08	0.06	0.08	0.08
700		0.08	0.08		
600		0.05	0.06	0.06	0.06

Table 2
Atomic ratio C/B in boron films deposited under various conditions

Temperature (°C)	Pressure (Pa)				
	20	50	100	200	300
1050	0.06				
1000	0.02	0.03	0.02	0.04	
900	0.02	0.02	0.05		
800	0.08	0.07	0.05	0.08	0.11
700		0.11	0.10		
600		0.05	0.11	0.11	0.12

and silicon contents were small, and atomic ratios of N/B and Si/B did not exceed 0.03 under all temperature and pressure conditions for deposition. The main component of N1s peak had a peak at 397.2–398.0 eV that could be assigned to be Si_3N_4 or BN [23]. A silicon component was detected only above 800°C, and the peak position was at 99.3–99.6 eV of metallic silicon. The source of silicon was probably the quartz glass substrate or the tube.

3.4. Surface morphology

All data presented above was from the films deposited with laser energy of 250 mJ/pulse. High laser energy is thought to introduce good crystallinity of the films, although splashing of the melt created by laser irradiation on the target often degrades the film surface morphology. In fact, we often observed micrometer-sized splashes or particles at laser energy of 250 mJ/pulse. Therefore, we studied the laser energy effect on the surface morphology to obtain crystallized boron film with a smoother surface.

Fig. 8 represents laser energy dependence on the surface morphology of boron films deposited at 900°C, 50 Pa by laser ablation. With the decrease of laser energy, the film morphology changed from films with irregular coarse particles on the surface (at 250 mJ/pulse), to smooth surfaces with a few embedded particulates (at 150 mJ/pulse), and aggregated particle structure (at 100 and 50 mJ/pulse). Fig. 9 depicts the corresponding XRD spectra of the films deposited under various laser energies. Films were kept in the crystallized form by decreasing laser energy from 250 to 100 mJ/pulse, though the films became amorphous when deposited at 50 mJ/pulse. Thus, crystallized boron film with a smoother surface was obtained at 150 mJ/pulse.

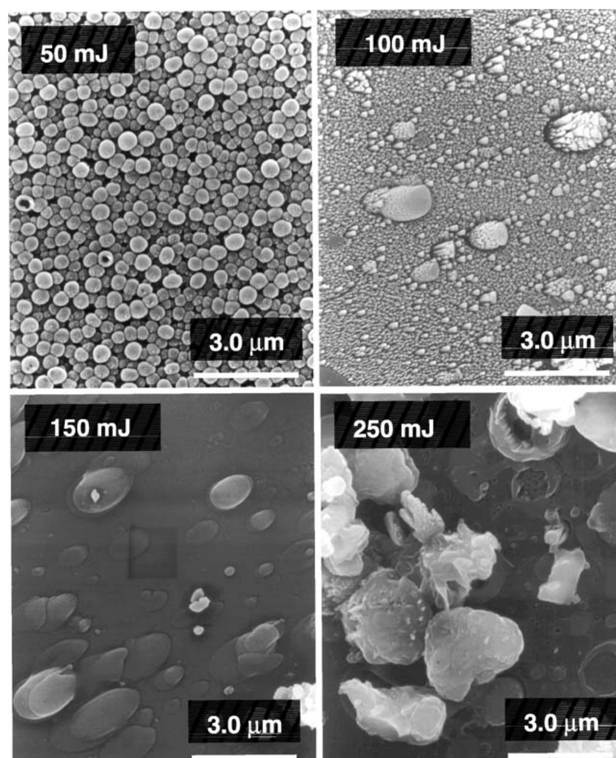

Fig. 8. Laser energy dependence on the surface morphology of boron films deposited at 900°C, 50 Pa by laser ablation.

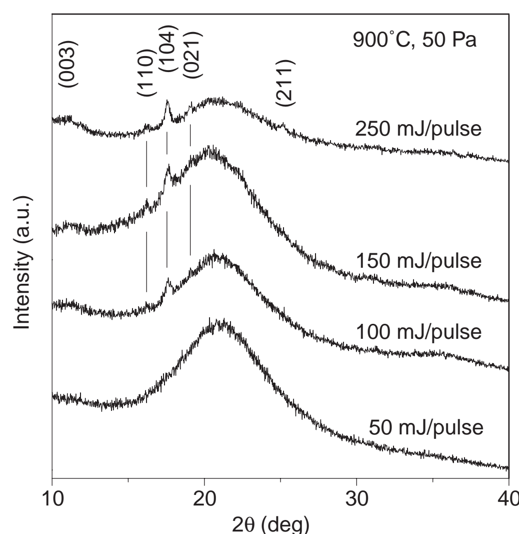

Fig. 9. Laser energy dependence on the XRD spectra of boron films deposited at 900°C, 50 Pa by laser ablation.

3.5. Growth mechanism

Crystallized boron films were fabricated at temperatures of 700°C to 1000°C and pressures of 50–300 Pa.

We first studied the substrate effect on the crystallinity of the boron films to clarify the growth mechanism. The crystalline films were always obtained irrespective of whether the substrate was single crystalline silicon, single crystalline sapphire, or amorphous quartz glass. This result suggested that gas phase nucleation was the main growth mechanism for the crystalline boron films.

Previously, we studied preparation of nanoparticle-aggregated films by laser ablation in the same pressure range as this experiment and found similar pressure dependences for cobalt oxide under the same configuration for deposition, without any substrate heating. The products were amorphous at low pressure of 1.33–6.65 Pa. With pressure increase, a crystalline film of Co_3O_4 (the same composition as the target) formed concurrently with nano-sized particulates at 13.3–266 Pa. Further pressure increases resulted in products with mixtures of Co_3O_4 and CoO, i.e., a less oxidized composition [26]. Such pressure dependence was true not only for simple oxides such as Co_3O_4, Fe_2O_3, and TiO_2, but also for complex oxides like $BaTiO_3$, $LaFeO_3$, $SrFeO_{3\text{-}x}$ [27,28], indicating that such pressure dependence is a general trend for laser ablation under off-axis configuration. However, the boundary pressures of the products and the particle size differed from material to material. The pressure range we examined for boron crystallized film preparation corresponded to the range where the product changed from amorphous to crystalline state, despite substrate temperatures being higher than in the previous studies. The background gas pressure affects the kinetic energy of the flying species in the plume due to the collision of ablated species including atoms, ions, molecules, particles, and clusters in the gas phase [18,20]. Above 10 Pa, most of the kinetic and internal energy of the ablation species is quenched by multiple collisions with the ambient gas on their journey from target to substrate [19]. Thus, the mobility of the atoms arriving at the substrate surface is effectively reduced at high pressure compared to that in low pressure [29] and vacuum [30]. The fabrication mechanism of crystallized boron films could mainly be based on the formation of crystalline nuclei or clusters of boron in the gas phase in the laser ablation plume. The cluster growth occurs only during the collisional expansion between the ablated species [31], and the collision processes play an important role in improving the crystalline nucleus/cluster formation in the laser ablation plume under suitable pressure conditions. Furthermore, the formation of B_n gas phase clusters (with $n>1$) might play an important role for promoting crystalline nucleus formation, if we take into account the many studies for carbon cluster formation at the initial stage of laser ablation and the strong tendency for boron to form icosahedral cluster unit of B_{12}. In fact, β-rhombohedral structure of boron is composed of these icosahedral cluster units, and thus the clusters could be the basic units to form the nuclei of the crystalline boron in the plume.

However, collision processes become less important at lower pressure (20 Pa), and the surface growth mechanism dominates the growth process, since the energy of deposits is not sufficiently dissipated. The boron oxide formation at low pressures with higher temperature (1000°C, 20 and 50 Pa) was assumed due to the reaction between energetic boron components spread on the substrate after landing, and residual oxygen molecules in the flowing gas. In fact as mentioned in Section 3.1, we performed similar experiments under UHV conditions with the same temperature range by substrate heating and found that it was extremely difficult to avoid boron oxide formation.

The temperature was another important parameter governing the crystallization of the boron film deposition from Fig. 4. We estimated the crystallinity of the boron films from the I_B/I_g XRD peak intensity ratio. Therefore, the ratio may increase with the film thickness. However, in our case, the proportion of crystallized phase increased with temperature based on TEM observation as described in Section 3.2. The most typical temperature effect is substrate temperature, if the crystallization process on the substrate governs the growth process [32,33]. However, this might not be true in our case, since the major crystallization process was considered to be governed by the gas-phase condensation. Another possibility is target temperature effect on ablation yield. In fact, ablation track on the target surface became deeper when the temperature was high, suggesting that the amount of ejected species was large. This leads to the increase in film thickness and the total amount of crystallites created in the gas phase. By this effect, we might be able to explain why the crystallite size of boron derived from XRD spectra did not increase with the temperature.

We also have to note that the crystallization temperature was relatively lower than that in the film preparation by the CVD method (generally above 1100°C). A crystallization temperature range of 700–1000°C in this study was similar to the case of crystallized boron nanobelt formation by laser ablation [22], and amorphous boron nanowire formation by sputtering [34]. Interestingly, all three cases were using physical deposition processes. Furthermore, oxygen contamination of these three products was relatively small, though the base pressures of the deposition chambers in these three studies were not UHV-grade, and oxygen leakage from the ambient was inevitable, leading to oxide formation. Boron is very reactive with oxygen, and forms B_2O_3 in equilibrium even with oxygen partial pressure of 6.8×10^{-22} Pa [35]. There should have been a removal process of B_2O_3, if once formed. The melting point of B_2O_3 is 450°C, and hence B_2O_3 exists in liquid phase within the temperature range

we tested. However, vaporization as a removal process will not proceed in this temperature range (equilibrium B_2O_3 vapor pressure is 9.7×10^{-8} Pa at 700°C, and 1.4×10^{-2} Pa at 1000°C [35]), especially after B_2O_3 is deposited on the substrate. The temperature in the plume could be much higher than the furnace temperature, and the vaporization might proceed in the plume. Furthermore, gaseous atomic boron produced by impinging ions or irradiating laser light could play an important role in B_2O_3 removal. Melted B_2O_3 would evaporate with the help of gaseous B in the following exothermic reaction ($\Delta G^\circ \approx -200$ kJ/mol) [35], and probably be removed from the system with simultaneous formation of solid boron:

$$B(g) + B_2O_3(l) \rightarrow B(s) + B_2O_3(g). \qquad (1)$$

Thus, boron films with less oxygen content were fabricated at relatively lower temperature using physical deposition processes.

4. Conclusion

Crystalline boron films were successfully fabricated by pulsed-laser ablation in temperatures from 700°C to 1000°C and pressures of 50–300 Pa. The crystallinity of boron films depended on the temperature and Ar pressure in a furnace. The films deposited at low temperature and low background gas pressure (below 700°C at 50 Pa, and below 1000°C at 20 Pa) consisted mainly of amorphous boron. The films were almost crystalline above 600°C at 50 Pa and the best crystallinity could be obtained at 1000°C, 100 Pa. The major contaminants in the deposited films were carbon and oxygen in crystalline films. A smoother surface can be obtained at 150 mJ/pulse. Film crystal structures exhibited no substrate dependence, suggesting that gas phase nucleation was the main mechanism for crystallization of boron films. The possible explanation for the effect of deposition conditions on the products was described.

Acknowledgments

One of the authors, Z. Wang, a JSPS fellow, is very grateful for the support from the Japan Society for the Promotion of Science.

References

[1] H. Werheit, Mater. Sci. Eng. B 29 (1995) 228–232.
[2] O.A. Golikova, Semiconductors 34 (2000) 363–366.
[3] K. Kamimura, T. Nagaoka, T. Shinomiya, M. Nakao, Y. Onuma, M. Makimura, Thin Solid Films 344 (1999) 342–344.
[4] Y. Kumashiro, T. Yokoyama, A. Sato, Y. Ando, J. Solid State Chem. 133 (1997) 314–321.
[5] D.M. Makowiecki, A.F. Jankowski, M.A. Mckernan, R.J. Foreman, J. Vac. Sci. Technol. A 8 (1990) 3910–3913.
[6] K. Nakamura, J. Electrochem. Soc. 131 (1984) 2691–2697.
[7] K. Kamimura, M. Ohkubo, T. Shinomiya, M. Nakao, Y. Onuma, J. Solid State Chem. 133 (1997) 100–103.
[8] L. Vandenbulckel, G. Vuillard, J. Electrochem. Soc. 124 (1977) 1938–1942.
[9] T. Sekine, N. Nakanishi, E. Kato, J. Jpn. Inst. Met. 53 (1989) 698–703.
[10] N.A. Sezgi, T. Dogu, H.O. Ozbelge, Ind. Eng. Chem. Res. 36 (1997) 5537–5540.
[11] E.A. Haupfear, L.D. Schmidt, Chem. Eng. Sci. 49 (1994) 2467–2481.
[12] N.A. Sezgi, A. Ersoy, T. Dogu, H.O. Ozbelge, Chem. Eng. Process. 40 (2001) 525–530.
[13] K. Kamimura, T. Yoshimura, T. Nagaoka, M. Nakao, Y. Onuma, M. Makimura, J. Solid State Chem. 154 (2000) 153–156.
[14] K. Kumashiro, K. Hirata, K. Sato, T. Yokoyama, T. Aisu, T. Ikeda, M. Minaguchi, J. Solid State Chem. 154 (2000) 26–32.
[15] N.A. Sezgi, T. Dogu, H.O. Ozbelge, Chem. Eng. Sci. 54 (1999) 3297–3304.
[16] J.T. Cheung, in: D.B. Chrisey, G.K. Hubler (Eds.), Pulsed Laser Deposition of Thin Films, Wiley Press, New York, 1994 (Chapter. 1).
[17] J.C. Miller, in: J.C. Miller, R.F. Haglund (Eds.), Laser Desorption and Ablation, Academic Press, San Diego, 1998 (Chapter. 1).
[18] R.K. Singh, J. Narayan, Phys. Rev. B 41 (1990) 8843–8859.
[19] P.R. Willmott, J.R. Huber, Rev. Mod. Phys. 72 (2000) 315–328.
[20] A.V. Gusarov, A.G. Gnedovets, I. Smurov, J. Appl. Phys. 88 (2000) 4352–4364.
[21] S.R. Franklin, R.K. Thareja, Appl. Surf. Sci. 177 (2001) 15–21.
[22] Z.K. Wang, Y. Shimizu, T. Sasaki, K. Kawaguchi, K. Kimura, N. Koshizaki, Chem. Phys. Lett. 368 (2003) 663–667.
[23] J.F. Moulder, W.F. Stickle, P.E. Sobol, K.D. Bomben, Handbook of X-ray Photoelectron Spectroscopy, Perkin-Elmer Corporation, Eden Prairie, 1992.
[24] C.J. Otten, O.R. Lourie, M.F. Yu, J.M. Cowley, M.J. Dyer, R.S. Ruoff, W.E. Buhro, J. Amer. Chem. Soc. 124 (2002) 4564–4565.
[25] W.C. Foo, J.S. Ozcomert, M. Trenary, Surf. Sci. 255 (1991) 245–258.
[26] N. Koshizaki, A. Narazaki, T. Sasaki, Scr. Mater. 44 (2001) 1925–1928.
[27] J.W. Yoon, T. Sasaki, N. Koshizaki, Appl. Phys. A 76 (2003) 641–643.
[28] Z.K. Wang, T. Sasaki, N. Koshizaki, J.J. Tunney, M.L. Post, Thin Solid Films 437 (2003) 95–100.
[29] K.H. Muller, Phys. Rev. B 35 (1987) 7906–7913.
[30] J. Gonzalo, R. Serna, J.M. Requejo, J. Solís, C.N. Afonso, A. Naudon, Appl. Surf. Sci. 154-155 (2000) 449–453.
[31] W. Marine, L. Patrone, B. Luk'yanchuk, M. Sentis, Appl. Surf. Sci. 154–155 (2000) 345–352.
[32] D.S. Misra, B.D. Padalia, S.P. Pai, R. Pinto, S.B. Palmer, Thin Solid Films 245 (1994) 186–190.
[33] O.G. Andrianov, S.O. Klimonsky, V.A. Kusikov, E.N. Lubin, Physica C 575 (1994) 235–240.
[34] L.M. Cao, Z. Zhang, L.L. Sun, C.X. Gao, M. He, Y.Q. Wang, Y.C. Li, X.Y. Zhang, G. Li, J. Zhang, W.K. Wang, Adv. Mater. 13 (2001) 1701–1704.
[35] D.D. Wagman, W.H. Evans, V.B. Parker, R.H. Schumm, I. Halow, B.S. Mailey, K.L. Churney, R.L. Nuttall, The NBS tables of chemical thermodynamic properties, selected values for inorganic and C1 and C2 organic substances in SI units, J. Phys. Chem. Ref. Data 2 (Suppl. 2) (1982) (Thermodynamic data).